Cell Reports

The Unique Cysteine of F-ATP Synthase OSCP Subunit Participates in Modulation of the Permeability Transition Pore

Graphical Abstract

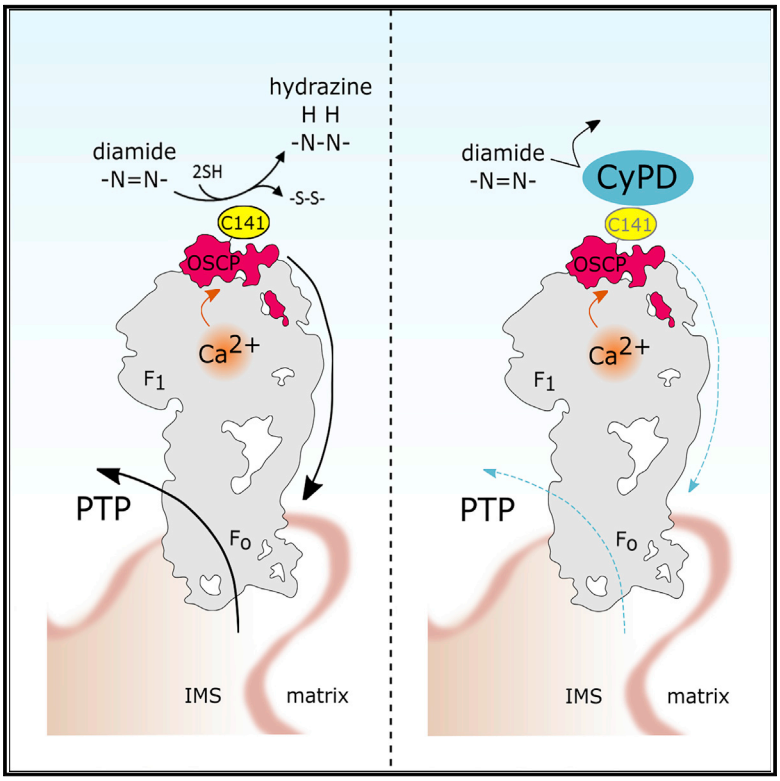

Highlights

- C141 of OSCP subunit of F-ATP synthase regulates the mitochondrial PTP
- Oxidation of OSCP C141 sensitizes the PTP to the inducing effect of diamide
- CyPD exerts a protecting effect by masking OSCP C141
- Genetic ablation of CyPD sensitizes PTP to diamide

Authors

Michela Carraro, Kristen Jones, Geppo Sartori, ..., Giorgio Arrigoni, Michael Forte, Paolo Bernardi

Correspondence

carraro.miche@gmail.com (M.C.), bernardi@bio.unipd.it (P.B.)

In Brief

The effect of oxidants on PTP opening has been widely reported, yet the targets are unknown. Here, Carraro et al. identify OSCP C141 of F-ATP synthase as a target of oxidants regulating the PTP. Cyclophilin D binding to OSCP has a protective effect and prevents PTP opening induced by oxidants.

Carraro et al., 2020, Cell Reports *32*, 108095
September 1, 2020
https://doi.org/10.1016/j.celrep.2020.108095

Cell Reports

CellPress
OPEN ACCESS

Report

The Unique Cysteine of F-ATP Synthase OSCP Subunit Participates in Modulation of the Permeability Transition Pore

Michela Carraro,[1,2,*] Kristen Jones,[3] Geppo Sartori,[1] Marco Schiavone,[1,2,7] Salvatore Antonucci,[1] Roza Kucharczyk,[4] Jean-Paul di Rago,[5] Cinzia Franchin,[1,6] Giorgio Arrigoni,[1,6] Michael Forte,[3] and Paolo Bernardi[1,2,8,*]

[1]Department of Biomedical Sciences, University of Padova, 35131 Padova, Italy
[2]Consiglio Nazionale delle Ricerche, Institute of Neuroscience, 35131 Padova, Italy
[3]Vollum Institute, OHSU, Portland, OR 97239, USA
[4]Institute of Biochemistry and Biophysics, Polish Academy of Sciences, 00-901 Warsaw, Poland
[5]Institut de Biochimie et Génétique Cellulaires and CNRS, UMR 5095, Université de Bordeaux, 33077 Bordeaux, France
[6]Proteomics Center, University of Padova and Azienda Ospedaliera di Padova, 35131 Padova, Italy
[7]Present address: Department of Molecular and Translational Medicine, University of Brescia, 25123 Brescia, Italy
[8]Lead Contact
*Correspondence: carraro.miche@gmail.com (M.C.), bernardi@bio.unipd.it (P.B.)
https://doi.org/10.1016/j.celrep.2020.108095

SUMMARY

The mitochondrial permeability transition pore (PTP) is a Ca^{2+}-activated channel that plays a key role in cell death. Thiol oxidation facilitates PTP opening, yet the targets and molecular mechanisms still await a definition. Here, we investigate the role of C141 of F-ATP synthase oligomycin sensitivity conferral protein (OSCP) subunit in PTP modulation by oxidation. We find that the OSCP C141S mutation confers resistance to PTP opening and cell death by diamide and MitoParaquat only when cyclophilin D (CyPD) has been ablated, a protective role that can be explained by CyPD shielding C141 from oxidants. The mutation decreases apoptosis in zebrafish embryos, indicating that this OSCP residue is involved in development. Site-directed mutagenesis in yeast suggests that other conserved cysteines in the α, γ, and c subunits of F-ATP synthase are not involved in PTP modulation. Thus, OSCP provides a strategic site that regulates PTP opening by the interplay between CyPD (un)binding and thiol oxidation-reduction.

INTRODUCTION

The permeability transition pore (PTP), or mitochondrial megachannel, is a Ca^{2+}-activated channel of the inner mitochondrial membrane that mediates permeabilization to solutes up to 1.5 kDa in a process defined permeability transition (PT) (Haworth and Hunter, 1979; Hunter and Haworth, 1979a, 1979b). The primary consequence of PTP opening is membrane depolarization. In case of long-lasting and stable openings, this is followed by matrix swelling, rupture of the outer membrane, and release of pro-apoptotic factors (Petronilli et al., 2001). Oxidation or cross-linking of thiol groups results in an increased open probability of the PTP (Petronilli et al., 1994), and this is exacerbated in many pathological conditions (Bernardi et al., 2015; Hurst et al., 2017; Szabó and Zoratti, 2014). Redox regulation involves at least three sites defined by careful phenotypic analysis of mammalian mitochondria after treatment with specific thiol reagents (Costantini et al., 1995a, 1995b, 1996, 1998; Petronilli et al., 1994, 2009). Two sites are accessible from the matrix side and protected by micromolar concentrations of N-ethylmaleimide, one being in apparent redox equilibrium with pyridine nucleotides and the other with glutathione (Costantini et al., 1996). The thiol cross-linkers phenylarsine oxide (PAO) and arsenite target the latter site, whereas reagents such as diamide (DIA) and *tert*-butylhydroperoxide (TBH) can react with both (Costantini et al., 1996). A distinct regulatory thiol appears to be located in the intermembrane space, where it reacts with copper-*o*-phenanthroline and millimolar concentrations of N-ethylmaleimide (Costantini et al., 1998). Understanding the redox mechanisms governing PTP opening would obviously benefit from a molecular definition of the PTP and of the identity of the reactive thiol groups.

The first candidate proposed for PTP formation is the inner membrane adenine nucleotide translocator (ANT), which in respiring mitochondria exchanges matrix ATP for cytosolic ADP (Duee and Vignais, 1965; Heldt and Klingenberg, 1965). This suggestion was based on the effects of atractylate (ATR) and bongkrekate (BKA), the selective inhibitors of ANT (Bruni and Luciani, 1962; Henderson and Lardy, 1970). While both reagents inhibit ATP/ADP exchange, ATR promotes while BKA inhibits the PT (Hunter and Haworth, 1979a). Binding of the inhibitors occurs at different sites and confers defined conformations to the ANT, the "c" state (nucleotide binding site facing the cytosol) induced by ATR and the "m" state (nucleotide binding

site facing the matrix) by BKA (Schultheiss and Klingenberg, 1984). Pore opening would be related to a Ca^{2+}-dependent conformational change of the ANT, which could be favored by binding of matrix cyclophilin D (CyPD) (Woodfield et al., 1998), possibly enhanced by cross-linking of C160 and C257 and decreased reactivity of C57 (McStay et al., 2002).

The second main candidate for PTP formation is the F-ATP synthase (Alavian et al., 2014; Bonora et al., 2013; Carraro et al., 2014; Giorgio et al., 2013; von Stockum et al., 2015), which has been recently characterized for its ability to generate Ca^{2+}-dependent, PTP-like channels in lipid bilayers or in giant liposomes reconstituted with highly purified enzyme preparations (Mnatsakanyan et al., 2019; Urbani et al., 2019). Although this function of F-ATP synthase is a matter of debate (Bernardi, 2020; Carraro et al., 2019; Carroll et al., 2019; He et al., 2017a, 2017b), a number of F-ATP synthase mutations do affect specific features of the PTP, considerably strengthening its proposed role in pore formation (Carraro et al., 2019; Gerle, 2016). Specifically, the PTP is affected by mutations of a highly conserved glycine residue of subunit c (Alavian et al., 2014), the T163S substitution of subunit β affecting Ca^{2+} sensitivity (Giorgio et al., 2017), the H135Q mutation of subunit oligomycin sensitivity conferral protein (OSCP) preventing pore inhibition by acidic pH (Antoniel et al., 2018), and mutations R107 of subunit g and R8 of subunit e that affect pore size and conductance (Guo et al., 2018, 2019).

In mammals, the best-defined PTP regulatory protein is CyPD (Amanakis et al., 2020; Javadov and Kuznetsov, 2013; Porter and Beutner, 2018), a matrix peptidyl prolyl *cis-trans* isomerase that favors pore opening (Broekemeier et al., 1989; Crompton et al., 1988; Fournier et al., 1987; Halestrap and Davidson, 1990; Nicolli et al., 1996). CyPD interacts with both ANT (Woodfield et al., 1998; McStay et al., 2002) and F-ATP synthase (Burstein et al., 2018; Gauba et al., 2017, 2019; Giorgio et al., 2013; Lee et al., 2016). Interestingly, C203 of CyPD confers PTP sensitivity to H_2O_2 (Nguyen et al., 2011), yet cells overexpressing CyPD are protected from killing by TBH (Lin and Lechleiter, 2002). Furthermore, in the absence of CyPD, the pore is still sensitive to oxidative stress (Basso et al., 2008), indicating that other cysteine residues participate in the redox modulation.

We are carrying out a systematic analysis of the role of individual cysteine residues of F-ATP synthase for their phenotypic effects on the PTP. Here, we report on the role of the unique cysteine of OSCP subunit in PTP modulation by oxidants in human cells and development of zebrafish embryos.

RESULTS

The PTP Is More Sensitive to DIA in the Absence of CyPD

CyPD is a "positive" modulator of the PTP. The absence of CyPD significantly desensitizes the pore to Ca^{2+}, resulting in inhibition (Baines et al., 2005; Basso et al., 2005; Nakagawa et al., 2005; Schinzel et al., 2005), yet CyPD overexpression protects from cell death induced by oxidative stress (Schubert and Grimm, 2004), in particular by TBH (Lin and Lechleiter, 2002). The molecular basis for such unexpected findings is still unknown and might be relevant to understand the regulatory mechanisms controlling PTP opening. To investigate this protective role of CyPD, we used wild-type and CyPD null mouse liver mitochondria (MLM) and tested the effect of DIA on the Ca^{2+} retention capacity (CRC), a measure of the sensitivity of the PTP to Ca^{2+} (Fontaine et al., 1998). In the absence of CyPD, the PTP was markedly desensitized to Ca^{2+}, but CyPD knockout (KO) mitochondria were much more sensitive to PTP opening by DIA (Figures 1A and 1B), an effect that was particularly clear when the data where normalized to the CRC/CRC_0 ratio (Figure 1C). These data suggest that CyPD counteracts the inducing effects of DIA on Ca^{2+}-dependent PTP opening. CyPD binds the OSCP subunit of F-ATP synthase; this interaction is favored by the acetylation of critical lysines (Lee et al., 2016) and inorganic phosphate (Pi) (Giorgio et al., 2009, 2013). OSCP possesses a unique cysteine, and we hypothesized that CyPD binding protects its thiol from redox modifications. To test this prediction, we evaluated the effect of DIA in wild-type mitochondria at both low (0.5 mM) and high Pi (5 mM) concentrations in order to modulate CyPD binding to OSCP. The PTP was extremely resistant to DIA at 5 mM Pi (i.e., under conditions of optimal CyPD binding), an effect that appears to be selective for DIA, because the inducing effect of PAO was not altered by Pi (Figure 1D). Interestingly, the substitution of Pi with vanadate (Vi) did not provide the same protection (Figure 1E), in line with the fact that binding of CyPD depends specifically on the presence of Pi, which cannot be replaced by Vi or arsenite (Basso et al., 2008). We next performed an immunoprecipitation of F-ATP synthase after treatment with DIA under nonreducing conditions both in wild-type and CyPD KO MLM. A low Pi concentration (0.5 mM) was used to minimize binding of CyPD to OSCP (Giorgio et al., 2009), thus ensuring accessibility of the OSCP subunit to DIA. The OSCP band at 23 kDa significantly decreased in a concentration-dependent manner (Figure 1F), possibly due to formation of a higher-molecular-weight complex, while the levels of subunits b and β were not significantly affected. These data strongly suggest that OSCP is one of the targets of DIA.

The OSCP C141S Mutation Protects against DIA-Induced PTP Opening and Cell Death in the Absence of CyPD

The unique cysteine of OSCP (C141 in the human protein) is located in the putative binding region of CyPD (Giorgio et al., 2013) in close proximity to H135 (Figure 2A), which mediates the PTP inhibitory response to acidic matrix pH (Antoniel et al., 2018). To test its role in PTP modulation, we generated HEK293 cells carrying the OSCP C141S mutation (clones 22 and 55). The mutation slightly decreased the expression of the OSCP protein, a potentially interesting observation that we are evaluating for further study (even though the decrease was not statistically significant), while no effect was observed for selected F-ATP synthase subunits (Figure 2B). Basal respiration, sensitivity to oligomycin, and maximal respiration were also not affected (Figure 2C). The sensitivity of the PTP to Ca^{2+} (Figure 2D), Cyclosporin (Cs) A (Figure 2E), and DIA (Figure 2F) was not changed. Based on the results obtained in MLM and C141S HEK293 cells, we reasoned that the phenotypic effect of the C141S mutation could be masked by CyPD binding. We therefore generated HEK293 cells carrying the OSCP C141S

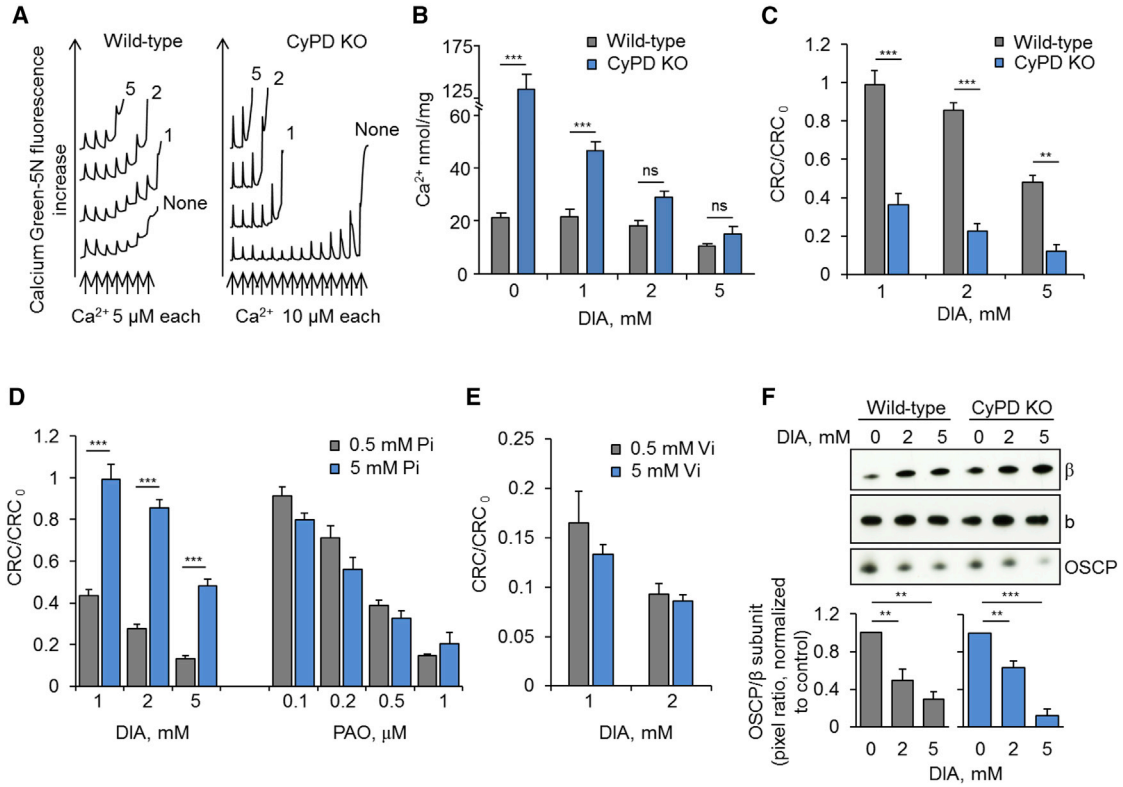

Figure 1. The PTP Is More Sensitive to DIA in the Absence of CyPD

(A–C) CRC assays with isolated MLM from wild-type and CyPD KO mice. (A) Representative traces where Ca^{2+} was added as indicated in the absence of DIA ("None") or in the presence of the DIA concentrations (mM) indicated on each trace. (B) Absolute values of CRC normalized to mitochondrial protein. (C) Normalized values of CRC, where CRC_0 is the CRC of mitochondria not treated with DIA. Histograms refer to the mean ± SEM of 11 (wild-type) or 3 (CyPD KO) independent experiments. ***p < 0.001 and **p < 0.01, two-way ANOVA.

(D) CRC assay with wild-type MLM in the presence of indicated concentrations of DIA and PAO at 0.5 mM and 5 mM Pi. Histograms refer to the CRC/CRC_0 ratio and are mean ± SEM of 11 (DIA) or 4 (PAO) independent experiments. ***p < 0.001, two-way ANOVA.

(E) CRC assays with wild-type MLM at 0.5 mM or 5 mM Vi in presence of indicated concentrations of DIA. Data are expressed as CRC/CRC_0 ratio and are mean ± SEM of three independent experiments.

(F) Wild-type and CyPD KO MLM were incubated in presence of 0.5 mM Pi with the indicated concentrations of DIA prior to solubilization with a digitonin-to-protein ratio of 1 g/g and subjected to the immunoprecipitation (IP) of F-ATP synthase (see details in STAR Methods). Subunits β, b and OSCP of F-ATP synthase were detected by western blot analysis. Histograms refer to OSCP/β pixel ratio at indicated concentrations of DIA normalized to the untreated condition (set as 1). Data are mean ± SEM of three independent experiments. ***p < 0.001 and **p < 0.01, one-way ANOVA.

mutation in a CyPD null (*Ppif*$^{-/-}$) genetic background (Figure 3A). The ablation of CyPD caused a significant rise in both basal and maximal respiration (Figures 3B and 3C). As previously observed (Giorgio et al., 2009), it also increased oligomycin-sensitive mitochondrial respiration (Figure 3D), while the combination with the OSCP C141S mutation reverted this phenotype. Strikingly, CyPD ablation unmasked the resistance of the OSCP C141S mutant to PTP induction by DIA (Figure 3E), unraveling the redox-sensitive role of this cysteine.

We next assessed cell viability upon treatment with different concentrations of DIA. The ablation of CyPD sensitized cells to oxidation, in particular to 0.5 mM DIA, while the combination with the OSCP C141S substitution could significantly prevent cell death (Figure 3F). Treatment with MitoParaquat (MitoPQ), which increases superoxide production within the matrix (Robb et al., 2015), caused the same cytotoxic effect in cells of all genotypes, while the protective effect of the C141S mutation became clear in the CyPD null cells (Figure 3G). Although DIA and MitoPQ modulate the PTP through OSCP C141, their effects are not completely prevented by the C > S substitution, indicating that the regulatory effect of oxidation cannot be entirely attributed to a single residue. Since other cysteines of the F-ATP synthase might contribute to this modulation, we carried out a site-directed mutagenesis study of conserved cysteines present in yeast F-ATP synthase subunits α, γ, and c and generated the corresponding C > S variants (Figures S1A and S1B). It has been previously shown that the yeast PTP matches the features of its mammalian counterpart, including sensitivity to oxidants (Carraro et al., 2014). Yeast C > S mutations that allow to fully retain the hydrolytic activity of the enzyme (Figure S2A) did not prevent the effect of DIA and PAO on PTP opening, as revealed by CRC assays in the presence of the Ca^{2+} ionophore ETH129 (Figures S2C–S2E). Interestingly, the ATP3 (γ) C117S mutant showed a significant resistance of the PTP to Ca^{2+}

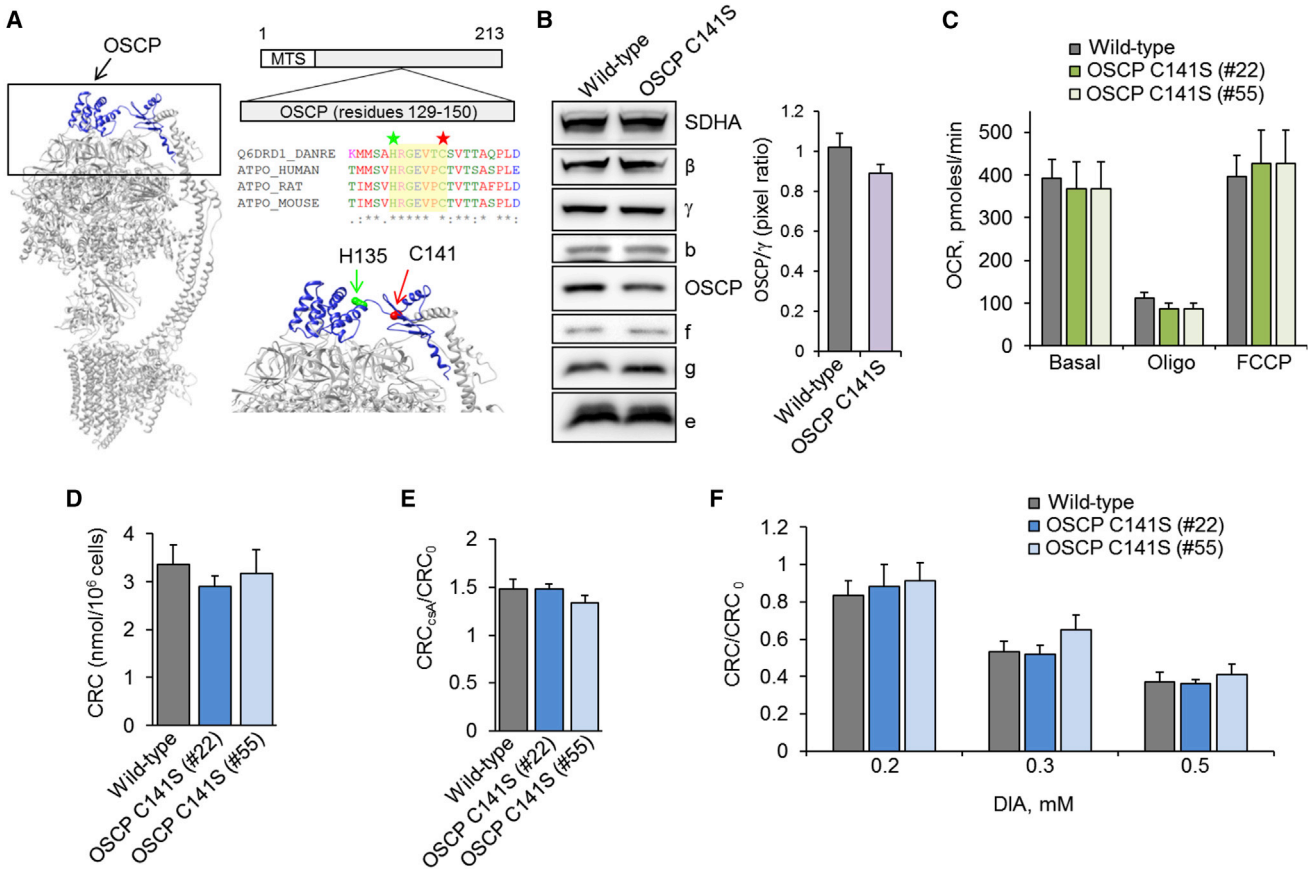

Figure 2. The OSCP C141S Mutation Does Not Affect Key Bioenergetics Features of HEK293 Cells

(A) F-ATP synthase structure (adapted from Gu et al., 2019) with the OSCP subunit highlighted in blue. Sequence alignment of zebrafish, human, rat, and mouse OSCP gene (residues 129–150 are shown). Positions of the C141 and the H135 are marked in the sequence alignment (red and green stars, respectively) and the structure.

(B) Western blot analysis of wild-type and OSCP C141S isolated mitochondria for indicated F-ATP synthase subunits. Histogram refers to the quantification of OSCP protein level respect to that of γ and represents the mean ± SEM of three independent blots.

(C) Mitochondrial respiration was assessed in live cells by Seahorse XF Analyzer upon stimulation with oligomycin (Oligo), FCCP (100 nM), and antimycin (AA) plus rotenone (R). Data are subtracted for AA+R-insensitive respiration (expressed as picomoles per minute) and are mean ± SEM of at least three independent experiments.

(D–F) CRC assay in permeabilized HEK293 cells in presence of 0.1 mM Pi. (D) Data are expressed as nmol $Ca^{2+}/10^6$ cells and are mean ± SEM of seven independent experiments. CRC assay in presence of CsA (E) or in the presence of indicated concentrations of DIA (F). Histograms refer to CRC/CRC_0 ratio and show the mean ± SEM of four (E) or three to six (F) independent experiments.

(Figure S2B). Taken together, these findings suggest that PTP modulation by oxidation in mammals may be affected by F-ATP synthase cysteines that are not shared with yeast.

To explore a possible molecular mechanism for the modulation of the PTP by OSCP C141, we performed an immunoprecipitation of OSCP under nonreducing conditions after incubation with DIA. The treatment increased the intensity of a protein complex of ~41 kDa in wild-type and CyPD KO mitochondria and at the same time decreased the OSCP signal at 23 kDa. This effect was completely prevented by the C141S substitution (Figure 3H), suggesting that treatment with DIA promotes the formation of a disulfide bond between OSCP and a partner protein. Analysis of the DIA-induced 41-kDa band by mass spectrometry revealed the presence of OSCP, which increased its abundance up to 30 times in the wild-type compared to the C141S mutant (Table S1). This finding suggests that DIA generates OSCP homodimers, possibly causing a structural rearrangement of F-ATP synthase that in turn may favor PTP opening.

The Expression of OSCP C138S Decreases Apoptosis in Zebrafish Embryos

Cell death is a critical process during the embryonic development of *Danio rerio* (zebrafish) (Prudent et al., 2015), and modulation of mitochondrial Ca^{2+} is one of its key regulators (Prudent et al., 2013). A contribution of PTP opening to zebrafish development was recently reported based on the finding that expression of the human T163S β subunit mutant of F-ATP synthase (which desensitizes the PTP to Ca^{2+}) strikingly decreases apoptosis in zebrafish embryos (Giorgio et al., 2017). Prompted by these observations, we tested whether

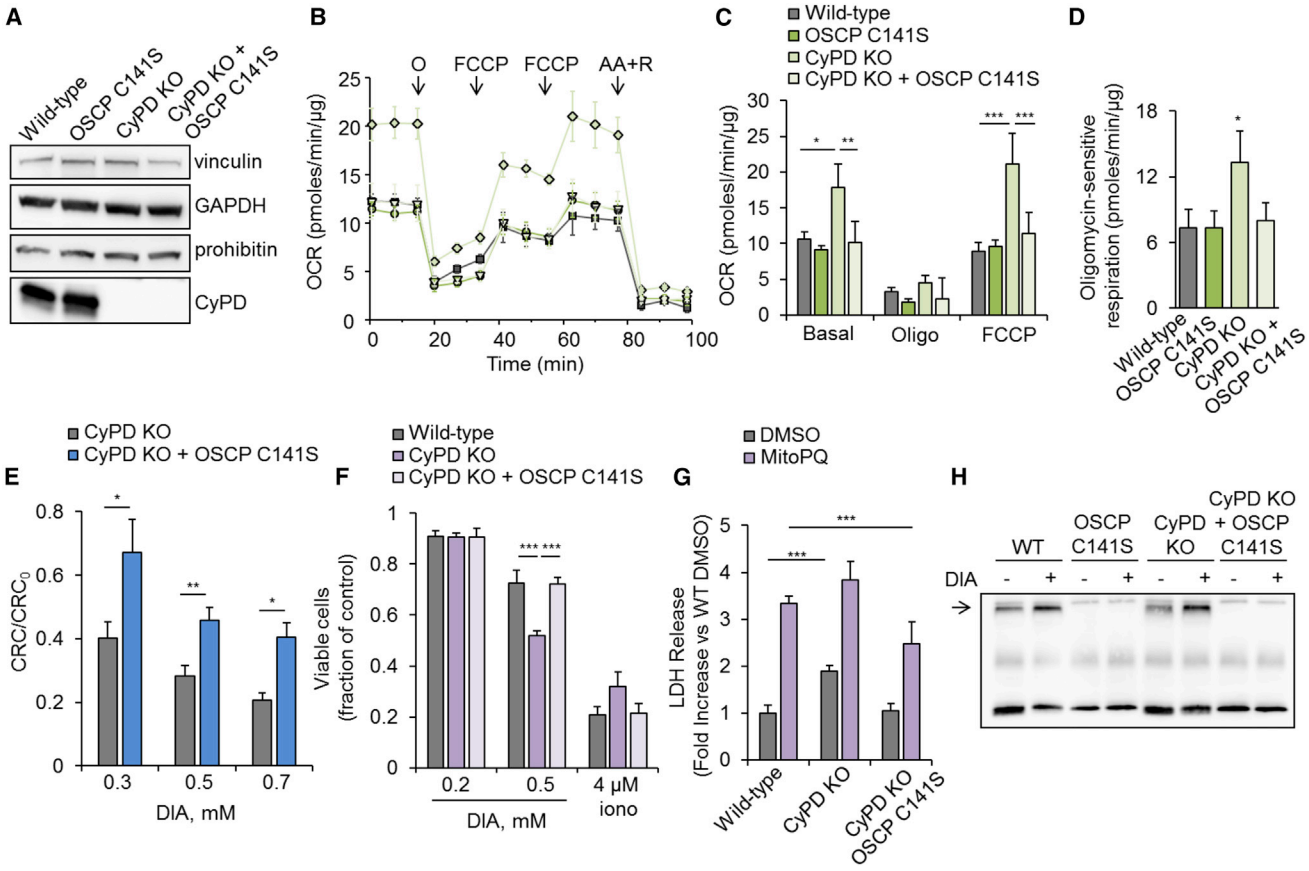

Figure 3. HEK293 OSCP C141S Cells Are Protected against DIA Toxicity in the Absence of CyPD

(A) Western blot analysis on lysates (40 µg each) of cells with the indicated genotypes.

(B–D) Mitochondrial respiration was evaluated in living cells by Seahorse XF Analyzer before and after the addition of oligomycin (Oligo), FCCP (100 nM), and antimycin (AA) plus rotenone (R). Representative traces of wild-type (squared symbol), OSCP C141S (rounded symbol), CyPD KO (rhomboid symbol), and CyPD KO + OSCP C141S (triangular symbol) are shown in (B), and OCR values (pmol/min) normalized for protein content (µg) and subtracted for AA+R respiration are shown in (C) and represent average ± SD of at least three independent experiments. *$p < 0.05$, **$p < 0.01$, and ***$p < 0.001$, two-way ANOVA. (D) Oligomycin-sensitive respiration expressed as mean ± SD of at least three independent experiments. *$p < 0.05$, one-way ANOVA, CyPD KO versus all other genotypes.

(E) CRC of permeabilized HEK293 cells in the presence of indicated concentrations of DIA. Data are expressed as ratio CRC/CRC_0 and are mean ± SEM of three to seven experiments. *$p < 0.05$ and **$p < 0.01$, Student's t test.

(F) Viable cells after treatment with the indicated concentrations of DIA and ionomycin. Values are normalized to untreated condition and are mean ± SEM of four independent experiments. ***$p < 0.001$, two-way ANOVA.

(G) Cell death analysis after treatment with 10 µM MitoPQ by means of LDH release. Values are normalized to those obtained in wild-type DMSO-treated cells. Data are mean ± SEM of three independent experiments. ***$p < 0.001$, two-way ANOVA.

(H) IP of OSCP from isolated mitochondria of the indicated genotypes upon treatment with 2 mM DIA. The 41-kDa band is indicated by the arrow. This western blot is representative of two independent experiments.

the OSCP cysteine might play a role in cell death *in vivo* by expressing wild-type or C138S (equivalent to the human C141) OSCP subunits in zebrafish embryos. Injection of constructs led to a similar expression of the protein, while the levels of endogenous γ subunit (used here as a marker of F-ATP synthase) were not affected (Figure 4A). Whole-mount immunofluorescence indicated that the expressed OSCP co-localized with mitochondrial TOM20 (Figure 4B). Remarkably, expression of the OSCP C138S construct increased the percentage of dead embryos at 24 hours post-fertilization (hpf) (Figure 4C). The expression of human OSCP C138S led to a decreased number of apoptotic nuclei at 72 hpf in the tail compared to controls (Figures 4D and 4E). These data support the notion that the unique OSCP cysteine, which we have shown to modulate PTP opening by oxidation, can be critical for the control of cell death in zebrafish development.

DISCUSSION

In this article, we investigated the role of the OSCP C141 in controlling PTP opening and found that it is a target of oxidation protected by CyPD binding. This cysteine appears to play a role in PTP-dependent cell death by DIA and MitoPQ and (to the extent that it is permissible to extrapolate our enforced-expression results) in zebrafish developmental apoptosis *in vivo*. The contribution of the F-ATP synthase to the formation and regulation of the

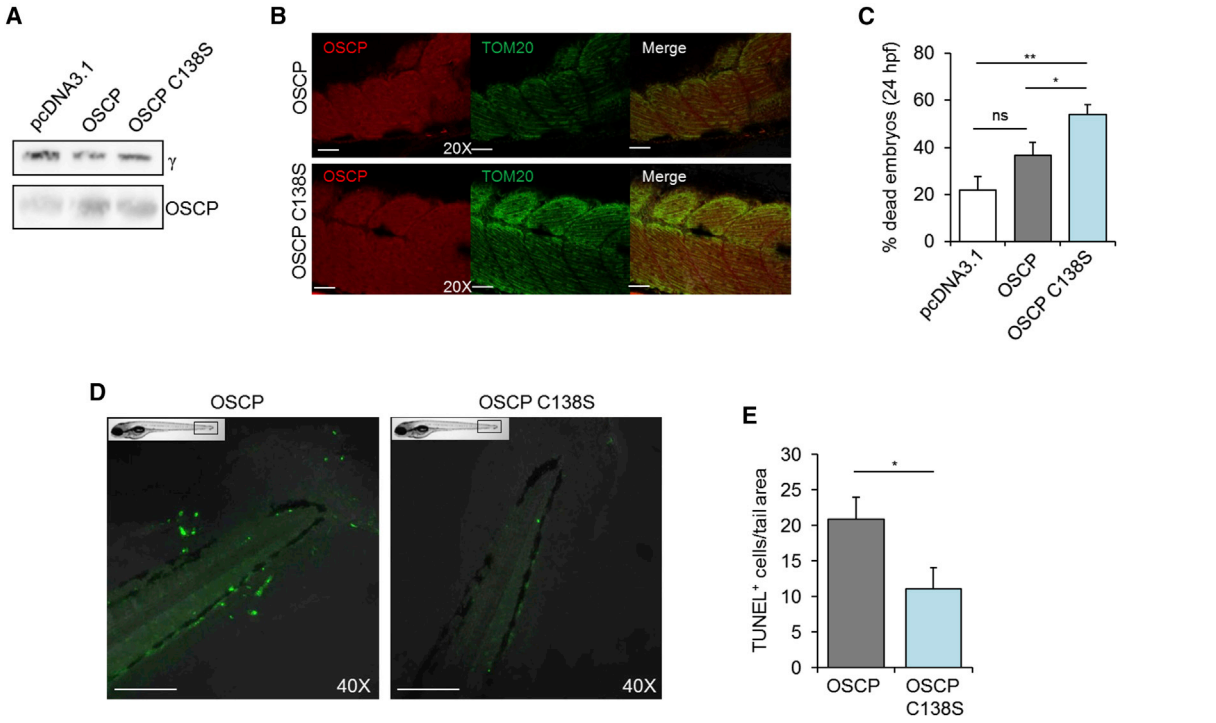

Figure 4. Expression of OSCP C138S Affects Cell Death in Zebrafish Embryos

Fertilized eggs at the one-cell stage were injected with empty, wild-type, or C138S OSCP pcDNA3.1 as described in STAR Methods. The number of injected embryos was between 40 and 100 for each experiment.

(A) Protein lysates from 72-hpf-injected embryos were analyzed by western blotting with antibodies against γ subunit and OSCP (one representative experiment out of three is shown). 30 μg of lysate was loaded for each sample.

(B) Injected embryos were subjected to immunofluorescence analysis using OSCP (red) and TOM20 (green) antibodies at 72 hpf (one representative staining out of three). Co-localization is reported in the merged panels.

(C) Dead embryos were counted 24 h post-injection. Data are expressed as percentage of dead embryos relative to the total number of injected embryos and represent mean ± SEM of six independent experiments. *$p < 0.05$ and **$p < 0.01$, Student's t test.

(D) Apoptosis was evaluated in 72-hpf embryos expressing wild-type or C138S OSCP by TUNEL assay. Representative full z stack images (40× objective) of the tail are shown. Apoptotic nuclei were visualized in green, while the tail is visible in bright field.

(E) The number of apoptotic nuclei was counted in the tail area (boxed in the larva miniature reported in the upper left corner). Selected area for analysis of wild-type and C138S-OSCP-injected embryos was 594,540 ± 112,432 and 589,090 ± 105,802 pixels, respectively. Data are mean ± SEM of six independent experiments (from three to six embryos per condition in each experiment, with a total number of 24 embryos analyzed per condition). *$p < 0.05$, Student's t test. Scale bars, 100 nm.

PTP is now supported by overwhelming evidence obtained both through site-directed mutagenesis (Alavian et al., 2014; Antoniel et al., 2018; Carraro et al., 2014; Giorgio et al., 2017; Guo et al., 2018, 2019) and through reconstitution of channel activity from highly purified preparations of the enzyme (Mnatsakanyan et al., 2019; Urbani et al., 2019). In particular, the OSCP subunit appears to be a key platform essential both for the modulation of the enzymatic catalysis (Murphy et al., 2019) and for PTP regulation by a variety of factors, including CyPD (Burstein et al., 2018; Gauba et al., 2017, 2019; Giorgio et al., 2013; Lee et al., 2016), the binding of which is a key event for the PTP response to Ca^{2+}. The unique H135 residue of OSCP, at the hinge region between the N- and C-terminal domains, confers PTP sensitivity to inhibition by H^+ (Antoniel et al., 2018). It is remarkable that OSCP C141, which is located in the same CyPD binding domain, confers PTP sensitization to oxidation by DIA only when CyPD is absent, providing an explanation to the long-standing observation that CyPD protects from TBH cytotoxicity (Lin and Lechleiter, 2002). A dual function for CyPD is also suggested by the finding that its upregulation promotes Ras-dependent tumorigenesis in a process that may involve p53 (Bigi et al., 2016).

The full molecular consequences of OSCP C141 oxidation by DIA remain to be clarified. Our findings indicate that a disulfide bridge forms between C141 of two OSCP subunits, consistent with the detection of OSCP at the position expected of a dimer after protein separation in nonreducing gels. F-ATP synthase dimers organize into long rows of oligomers that contribute to shape the curvature of the cristae (Baker et al., 2012; Blum et al., 2019; Davies et al., 2012; Jiko et al., 2015). Considering the angle of ~90° between monomers in the V-shaped F-ATP synthase (Kühlbrandt, 2019), an interaction between OSCP subunits facing one another appears impossible, as the distance is far above the minimum of ~2 Å required for disulfide bridge formation. A lateral interaction with the neighboring units in the oligomer appears unlikely, so we suspect that the interaction takes place in OSCP subunits belonging to adjacent

cristae. Cysteine oxidation leads to not only the possible generation of disulfide bridges but also the conversion into sulfenic, sulfinic, and sulfonic acid or a nitrosothiol (Poole, 2015), expanding the range of possible oxidative modifications with effects that are difficult to predict. It should also be considered that many thiol groups might orchestrate the effect of oxidation on the PTP and that these sites can belong to other subunits of the F-ATP synthase and/or other PTP-related proteins. Indeed, the absence of the OSCP C141 did not fully prevent the effect of oxidation on PTP opening, and this clearly indicates that a cooperation among redox sites must occur. The site-mutagenesis study carried out in yeast indicates that the conserved cysteines in subunits α, γ, and c are probably not the best candidates for such cooperation. It is of note that most of the unique cysteine residues of *Homo sapiens* are located in the b, d, f, and A6L subunits of the peripheral stalk, for which a key role in the mechanism of PTP formation has been proposed (Giorgio et al., 2018).

It should also be kept in mind that other pathways for mitochondrial permeabilization to Ca^{2+} exist and that a prominent case can be made for the ANT. The ANT can form Ca^{2+}-activated channels with conductance up to 0.6 nS inhibited by BKA and CsA (Brustovetsky and Klingenberg, 1996; Brustovetsky et al., 2002). An ANT-like channel could be detected in patch-clamp studies of mitoplasts in the absence of an assembled F-ATP synthase (Neginskaya et al., 2019), suggesting that the ANT may contribute to the PT, possibly through oxidative modifications that could be overshadowed by F-ATP synthase/PTP formation in wild-type mitochondria. Indeed, two ANT cysteines (C160 and C257) can react with PAO and DIA, forming intramolecular cross-links directly or via glutathione, respectively, while activating pore opening (McStay et al., 2002), but whether a causal relationship exists has not been established. Copper-*o*-phenanthroline has also been proposed to induce PTP opening through ANT dimerization by cross-linking of C56 (McStay et al., 2002), yet the PTP could be induced by this reagent without dimerization of the ANT (Costantini et al., 1998). Finally, ablation of ANT isoforms 1 and 2 did not prevent the effect of oxidants on the PTP, which still responded to DIA and H_2O_2 (Kokoszka et al., 2004). We think that whether ANT cysteines contribute to CsA-sensitive permeabilization by oxidants should be assessed by site-directed mutagenesis.

In spite of the remarkable effect of oxidants on the PTP, no cysteine mutations in candidate PTP constituents had ever been reported. The effect of the OSCP subunit C141S mutation characterized here is therefore the first example of PTP modulation by a specific cysteine residue. Remarkably, OSCP C141 is shielded by the main PTP "activator" CyPD, for which we have revealed a somewhat unexpected protective role that, however, nicely fits protection from TBH-induced cell death by CyPD overexpression (Lin and Lechleiter, 2002). These findings uncover a sophisticated interplay between the inducing and protective effects of this mitochondrial chaperone. It should be stressed that the C141S mutant cells are perfectly functional, allowing firm conclusions to be made about the specific role of C141 of OSCP in PTP modulation. Thus, this finding contributes to the ongoing debate on the nature of the PTP and a mechanistic understanding of the transition of F-ATP synthase from an energy-conserving to an energy-dissipating device.

STAR★METHODS

Detailed methods are provided in the online version of this paper and include the following:

- KEY RESOURCES TABLE
- RESOURCE AVAILABILITY
  - Lead Contact
  - Materials Availability
  - Data and Code Availability
- EXPERIMENTAL MODEL AND SUBJECT DETAILS
  - HEK293 cells
  - Mice
  - Zebrafish
- METHOD DETAILS
  - Generation of HEK293 OSCP C141S and CyPD KO cell lines
  - Injection of zebrafish embryos
  - Generation of yeast C > S mutants
  - Preparation of isolated mitochondria from HEK293 cells, mouse liver, and yeast
  - Ca^{2+} Retention Capacity (CRC)
  - ATP hydrolysis
  - Oxygen consumption rate
  - Immunoprecipitation and Western Blot
  - In-gel trypsin digestion and LC-MS/MS analysis
  - Cell death assay (LDH release)
  - Cell viability assay (MTS test)
  - Whole-mount immunofluorescence
  - TdT-mediated dUTP Nick-End Labeling (TUNEL) assay
- QUANTIFICATION AND STATISTICAL ANALYSIS

SUPPLEMENTAL INFORMATION

Supplemental Information can be found online at https://doi.org/10.1016/j.celrep.2020.108095.

ACKNOWLEDGMENTS

This research was funded by the Italian Association for Cancer Research (AIRC; grant IG17067), Fondation Leducq (16CVD04), and the Ministry for the University and Research, Italy (2017LHFW42).

AUTHOR CONTRIBUTIONS

Conceptualization, M.C., M.F., and P.B.; Methodology, M.C., K.J., M.S., S.A., C.F., G.A., R.K., and J.-P.d.R.; Formal Analysis, M.C., M.S., S.A., C.F., and G.A.; Investigation, M.C., K.J., M.S., S.A., and C.F.; Resources, G.A., M.F., and P.B.; Writing—Original Draft, M.C. and P.B.; Writing—Review & Editing, M.C. and P.B.; Supervision, G.A., M.F., and P.B.; Funding Acquisition, G.A., M.F., and P.B. All authors have read and agreed to the published version of the manuscript.

DECLARATION OF INTERESTS

The authors declare no competing interests.

Received: April 15, 2020
Revised: July 13, 2020
Accepted: August 10, 2020
Published: September 1, 2020

REFERENCES

Alavian, K.N., Beutner, G., Lazrove, E., Sacchetti, S., Park, H.A., Licznerski, P., Li, H., Nabili, P., Hockensmith, K., Graham, M., et al. (2014). An uncoupling channel within the c-subunit ring of the F_1F_O ATP synthase is the mitochondrial permeability transition pore. Proc. Natl. Acad. Sci. USA *111*, 10580–10585.

Amanakis, G., Sun, J., Fergusson, M.M., McGinty, S., Liu, C., Molkentin, J.D., and Murphy, E. (2020). Cysteine 202 of cyclophilin D is a site of multiple post-translational modifications and plays a role in cardioprotection. Cardiovasc. Res. Published online March 4, 2020. https://doi.org/10.1093/cvr/cvaa053.

Antoniel, M., Jones, K., Antonucci, S., Spolaore, B., Fogolari, F., Petronilli, V., Giorgio, V., Carraro, M., Di Lisa, F., Forte, M., et al. (2018). The unique histidine in OSCP subunit of F-ATP synthase mediates inhibition of the permeability transition pore by acidic pH. EMBO Rep. *19*, 257–268.

Baines, C.P., Kaiser, R.A., Purcell, N.H., Blair, N.S., Osinska, H., Hambleton, M.A., Brunskill, E.W., Sayen, M.R., Gottlieb, R.A., Dorn, G.W., et al. (2005). Loss of cyclophilin D reveals a critical role for mitochondrial permeability transition in cell death. Nature *434*, 658–662.

Baker, L.A., Watt, I.N., Runswick, M.J., Walker, J.E., and Rubinstein, J.L. (2012). Arrangement of subunits in intact mammalian mitochondrial ATP synthase determined by cryo-EM. Proc. Natl. Acad. Sci. USA *109*, 11675–11680.

Basso, E., Fante, L., Fowlkes, J., Petronilli, V., Forte, M.A., and Bernardi, P. (2005). Properties of the permeability transition pore in mitochondria devoid of cyclophilin D. J. Biol. Chem. *280*, 18558–18561.

Basso, E., Petronilli, V., Forte, M.A., and Bernardi, P. (2008). Phosphate is essential for inhibition of the mitochondrial permeability transition pore by cyclosporin A and by cyclophilin D ablation. J. Biol. Chem. *283*, 26307–26311.

Bernardi, P. (2020). Mechanisms for Ca^{2+}-dependent permeability transition in mitochondria. Proc. Natl. Acad. Sci. USA *117*, 2743–2744.

Bernardi, P., Rasola, A., Forte, M., and Lippe, G. (2015). The mitochondrial permeability transition pore: Channel formation by F-ATP synthase, integration in signal transduction, and role in pathophysiology. Physiol. Rev. *95*, 1111–1155.

Bietenhader, M., Martos, A., Tetaud, E., Aiyar, R.S., Sellem, C.H., Kucharczyk, R., Clauder-Münster, S., Giraud, M.F., Godard, F., Salin, B., et al. (2012). Experimental relocation of the mitochondrial ATP9 gene to the nucleus reveals forces underlying mitochondrial genome evolution. PLoS Genet. *8*, e1002876.

Bigi, A., Beltrami, E., Trinei, M., Stendardo, M., Pelicci, P.G., and Giorgio, M. (2016). Cyclophilin D counteracts P53-mediated growth arrest and promotes Ras tumorigenesis. Oncogene *35*, 5132–5143.

Blum, T.B., Hahn, A., Meier, T., Davies, K.M., and Kühlbrandt, W. (2019). Dimers of mitochondrial ATP synthase induce membrane curvature and self-assemble into rows. Proc. Natl. Acad. Sci. USA *116*, 4250–4255.

Bonneaud, N., Ozier-Kalogeropoulos, O., Li, G.Y., Labouesse, M., Minvielle-Sebastia, L., and Lacroute, F. (1991). A family of low and high copy replicative, integrative and single-stranded *S. cerevisiae/E. coli* shuttle vectors. Yeast *7*, 609–615.

Bonnefoy, N., and Fox, T.D. (2001). Genetic transformation of *Saccharomyces cerevisiae* mitochondria. Methods Cell Biol. *65*, 381–396.

Bonora, M., Bononi, A., De Marchi, E., Giorgi, C., Lebiedzinska, M., Marchi, S., Patergnani, S., Rimessi, A., Suski, J.M., Wojtala, A., et al. (2013). Role of the c subunit of the F_O ATP synthase in mitochondrial permeability transition. Cell Cycle *12*, 674–683.

Broekemeier, K.M., Dempsey, M.E., and Pfeiffer, D.R. (1989). Cyclosporin A is a potent inhibitor of the inner membrane permeability transition in liver mitochondria. J. Biol. Chem. *264*, 7826–7830.

Bruni, A., and Luciani, S. (1962). Effects of atractyloside and oligomycin on magnesium-stimulated adenosine triphosphatase and on adenosine triphosphate-induced contraction of swollen mitochondria. Nature *196*, 578–580.

Brustovetsky, N., and Klingenberg, M. (1996). Mitochondrial ADP/ATP carrier can be reversibly converted into a large channel by Ca^{2+}. Biochemistry *35*, 8483–8488.

Brustovetsky, N., Tropschug, M., Heimpel, S., Heidkämper, D., and Klingenberg, M. (2002). A large Ca^{2+}-dependent channel formed by recombinant ADP/ATP carrier from *Neurospora crassa* resembles the mitochondrial permeability transition pore. Biochemistry *41*, 11804–11811.

Burstein, S.R., Kim, H.J., Fels, J.A., Qian, L., Zhang, S., Zhou, P., Starkov, A.A., Iadecola, C., and Manfredi, G. (2018). Estrogen receptor beta modulates permeability transition in brain mitochondria. Biochim. Biophys. Acta Bioenerg. *1859*, 423–433.

Carraro, M., Giorgio, V., Šileikytė, J., Sartori, G., Forte, M., Lippe, G., Zoratti, M., Szabò, I., and Bernardi, P. (2014). Channel formation by yeast F-ATP synthase and the role of dimerization in the mitochondrial permeability transition. J. Biol. Chem. *289*, 15980–15985.

Carraro, M., Checchetto, V., Szabó, I., and Bernardi, P. (2019). F-ATP synthase and the permeability transition pore: fewer doubts, more certainties. FEBS Lett. *593*, 1542–1553.

Carroll, J., He, J., Ding, S., Fearnley, I.M., and Walker, J.E. (2019). Persistence of the permeability transition pore in human mitochondria devoid of an assembled ATP synthase. Proc. Natl. Acad. Sci. USA *116*, 12816–12821.

Costantini, P., Chernyak, B.V., Petronilli, V., and Bernardi, P. (1995a). Selective inhibition of the mitochondrial permeability transition pore at the oxidation-reduction sensitive dithiol by monobromobimane. FEBS Lett. *362*, 239–242.

Costantini, P., Petronilli, V., Colonna, R., and Bernardi, P. (1995b). On the effects of paraquat on isolated mitochondria. Evidence that paraquat causes opening of the cyclosporin A-sensitive permeability transition pore synergistically with nitric oxide. Toxicology *99*, 77–88.

Costantini, P., Chernyak, B.V., Petronilli, V., and Bernardi, P. (1996). Modulation of the mitochondrial permeability transition pore by pyridine nucleotides and dithiol oxidation at two separate sites. J. Biol. Chem. *271*, 6746–6751.

Costantini, P., Colonna, R., and Bernardi, P. (1998). Induction of the mitochondrial permeability transition by N-ethylmaleimide depends on secondary oxidation of critical thiol groups. Potentiation by copper-*ortho*-phenanthroline without dimerization of the adenine nucleotide translocase. Biochim. Biophys. Acta *1365*, 385–392.

Cox, J., and Mann, M. (2008). MaxQuant enables high peptide identification rates, individualized p.p.b.-range mass accuracies and proteome-wide protein quantification. Nat. Biotechnol. *26*, 1367–1372.

Crompton, M., Ellinger, H., and Costi, A. (1988). Inhibition by cyclosporin A of a Ca^{2+}-dependent pore in heart mitochondria activated by inorganic phosphate and oxidative stress. Biochem. J. *255*, 357–360.

Davies, K.M., Anselmi, C., Wittig, I., Faraldo-Gómez, J.D., and Kühlbrandt, W. (2012). Structure of the yeast F_1F_o-ATP synthase dimer and its role in shaping the mitochondrial cristae. Proc. Natl. Acad. Sci. USA *109*, 13602–13607.

Di Lisa, F., Menabò, R., Canton, M., Barile, M., and Bernardi, P. (2001). Opening of the mitochondrial permeability transition pore causes depletion of mitochondrial and cytosolic NAD^+ and is a causative event in the death of myocytes in postischemic reperfusion of the heart. J. Biol. Chem. *276*, 2571–2575.

Duee, E.D., and Vignais, P.V. (1965). Echange entre adenine-nucleotides extra- et intramitochondriaux. Biochim. Biophys. Acta *107*, 184–188.

Fontaine, E., Ichas, F., and Bernardi, P. (1998). A ubiquinone-binding site regulates the mitochondrial permeability transition pore. J. Biol. Chem. *273*, 25734–25740.

Fournier, N., Ducet, G., and Crevat, A. (1987). Action of cyclosporine on mitochondrial calcium fluxes. J. Bioenerg. Biomembr. *19*, 297–303.

Gauba, E., Guo, L., and Du, H. (2017). Cyclophilin D promotes brain mitochondrial F1FO ATP synthase dysfunction in aging mice. J. Alzheimers Dis. *55*, 1351–1362.

Gauba, E., Chen, H., Guo, L., and Du, H. (2019). Cyclophilin D deficiency attenuates mitochondrial F1Fo ATP synthase dysfunction via OSCP in Alzheimer's disease. Neurobiol. Dis. *121*, 138–147.

Gerle, C. (2016). On the structural possibility of pore-forming mitochondrial F_oF_1 ATP synthase. Biochim. Biophys. Acta *1857*, 1191–1196.

Giorgio, V., Bisetto, E., Soriano, M.E., Dabbeni-Sala, F., Basso, E., Petronilli, V., Forte, M.A., Bernardi, P., and Lippe, G. (2009). Cyclophilin D modulates

mitochondrial F_0F_1-ATP synthase by interacting with the lateral stalk of the complex. J. Biol. Chem. *284*, 33982–33988.

Giorgio, V., von Stockum, S., Antoniel, M., Fabbro, A., Fogolari, F., Forte, M., Glick, G.D., Petronilli, V., Zoratti, M., Szabó, I., et al. (2013). Dimers of mitochondrial ATP synthase form the permeability transition pore. Proc. Natl. Acad. Sci. USA *110*, 5887–5892.

Giorgio, V., Burchell, V., Schiavone, M., Bassot, C., Minervini, G., Petronilli, V., Argenton, F., Forte, M., Tosatto, S., Lippe, G., and Bernardi, P. (2017). Ca^{2+} binding to F-ATP synthase β subunit triggers the mitochondrial permeability transition. EMBO Rep. *18*, 1065–1076.

Giorgio, V., Guo, L., Bassot, C., Petronilli, V., and Bernardi, P. (2018). Calcium and regulation of the mitochondrial permeability transition. Cell Calcium *70*, 56–63.

Godard, F., Tetaud, E., Duvezin-Caubet, S., and di Rago, J.P. (2011). A genetic screen targeted on the FO component of mitochondrial ATP synthase in Saccharomyces cerevisiae. J. Biol. Chem. *286*, 18181–18189.

Gu, J., Zhang, L., Zong, S., Guo, R., Liu, T., Yi, J., Wang, P., Zhuo, W., and Yang, M. (2019). Cryo-EM structure of the mammalian ATP synthase tetramer bound with inhibitory protein IF1. Science *364*, 1068–1075.

Guo, L., Carraro, M., Sartori, G., Minervini, G., Eriksson, O., Petronilli, V., and Bernardi, P. (2018). Arginine 107 of yeast ATP synthase subunit g mediates sensitivity of the mitochondrial permeability transition to phenylglyoxal. J. Biol. Chem. *293*, 14632–14645.

Guo, L., Carraro, M., Carrer, A., Minervini, G., Urbani, A., Masgras, I., Tosatto, S.C.E., Szabò, I., Bernardi, P., and Lippe, G. (2019). Arg-8 of yeast subunit e contributes to the stability of F-ATP synthase dimers and to the generation of the full-conductance mitochondrial megachannel. J. Biol. Chem. *294*, 10987–10997.

Halestrap, A.P., and Davidson, A.M. (1990). Inhibition of $Ca^{2(+)}$-induced large-amplitude swelling of liver and heart mitochondria by cyclosporin is probably caused by the inhibitor binding to mitochondrial-matrix peptidyl-prolyl *cis-trans* isomerase and preventing it interacting with the adenine nucleotide translocase. Biochem. J. *268*, 153–160.

Haworth, R.A., and Hunter, D.R. (1979). The Ca^{2+}-induced membrane transition in mitochondria. II. Nature of the Ca^{2+} trigger site. Arch. Biochem. Biophys. *195*, 460–467.

He, J., Carroll, J., Ding, S., Fearnley, I.M., and Walker, J.E. (2017a). Permeability transition in human mitochondria persists in the absence of peripheral stalk subunits of ATP synthase. Proc. Natl. Acad. Sci. USA *114*, 9086–9091.

He, J., Ford, H.C., Carroll, J., Ding, S., Fearnley, I.M., and Walker, J.E. (2017b). Persistence of the mitochondrial permeability transition in the absence of subunit c of human ATP synthase. Proc. Natl. Acad. Sci. USA *114*, 3409–3414.

Heldt, H.W., and Klingenberg, M. (1965). Endogenous nucleotides of mitochondria participating in phosphate transfer reactions as studied with 32P labelled orthophosphate and ultramicro scale ion exchange chromatography. Biochem. Z. *343*, 433–451.

Henderson, P.J., and Lardy, H.A. (1970). Bongkrekic acid. An inhibitor of the adenine nucleotide translocase of mitochondria. J. Biol. Chem. *245*, 1319–1326.

Hunter, D.R., and Haworth, R.A. (1979a). The Ca^{2+}-induced membrane transition in mitochondria. I. The protective mechanisms. Arch. Biochem. Biophys. *195*, 453–459.

Hunter, D.R., and Haworth, R.A. (1979b). The Ca^{2+}-induced membrane transition in mitochondria. III. Transitional Ca^{2+} release. Arch. Biochem. Biophys. *195*, 468–477.

Hurst, S., Hoek, J., and Sheu, S.S. (2017). Mitochondrial Ca^{2+} and regulation of the permeability transition pore. J. Bioenerg. Biomembr. *49*, 27–47.

Javadov, S., and Kuznetsov, A. (2013). Mitochondrial permeability transition and cell death: the role of cyclophilin d. Front. Physiol. *4*, 76.

Jiko, C., Davies, K.M., Shinzawa-Itoh, K., Tani, K., Maeda, S., Mills, D.J., Tsukihara, T., Fujiyoshi, Y., Kühlbrandt, W., and Gerle, C. (2015). Bovine F1Fo ATP synthase monomers bend the lipid bilayer in 2D membrane crystals. eLife *4*, e06119.

Kokoszka, J.E., Waymire, K.G., Levy, S.E., Sligh, J.E., Cai, J., Jones, D.P., MacGregor, G.R., and Wallace, D.C. (2004). The ADP/ATP translocator is not essential for the mitochondrial permeability transition pore. Nature *427*, 461–465.

Kühlbrandt, W. (2019). Structure and mechanisms of F-type ATP synthases. Annu. Rev. Biochem. *88*, 515–549.

Lee, C.F., Chavez, J.D., Garcia-Menendez, L., Choi, Y., Roe, N.D., Chiao, Y.A., Edgar, J.S., Goo, Y.A., Goodlett, D.R., Bruce, J.E., and Tian, R. (2016). Normalization of NAD^+ Redox Balance as a Therapy for Heart Failure. Circulation *134*, 883–894.

Lin, D.T., and Lechleiter, J.D. (2002). Mitochondrial targeted cyclophilin D protects cells from cell death by peptidyl prolyl isomerization. J. Biol. Chem. *277*, 31134–31141.

McStay, G.P., Clarke, S.J., and Halestrap, A.P. (2002). Role of critical thiol groups on the matrix surface of the adenine nucleotide translocase in the mechanism of the mitochondrial permeability transition pore. Biochem. J. *367*, 541–548.

Mnatsakanyan, N., Llaguno, M.C., Yang, Y., Yan, Y., Weber, J., Sigworth, F.J., and Jonas, E.A. (2019). A mitochondrial megachannel resides in monomeric F_1F_O ATP synthase. Nat. Commun. *10*, 5823.

Murphy, B.J., Klusch, N., Langer, J., Mills, D.J., Yildiz, Ö., and Kühlbrandt, W. (2019). Rotary substates of mitochondrial ATP synthase reveal the basis of flexible F1-FO coupling. Science *364*, eaaw9128.

Nakagawa, T., Shimizu, S., Watanabe, T., Yamaguchi, O., Otsu, K., Yamagata, H., Inohara, H., Kubo, T., and Tsujimoto, Y. (2005). Cyclophilin D-dependent mitochondrial permeability transition regulates some necrotic but not apoptotic cell death. Nature *434*, 652–658.

Neginskaya, M.A., Solesio, M.E., Berezhnaya, E.V., Amodeo, G.F., Mnatsakanyan, N., Jonas, E.A., and Pavlov, E.V. (2019). ATP synthase C-subunit-deficient mitochondria have a small cyclosporine A-sensitive channel, but lack the permeability transition pore. Cell Rep. *26*, 11–17.e2.

Nguyen, T.T., Stevens, M.V., Kohr, M., Steenbergen, C., Sack, M.N., and Murphy, E. (2011). Cysteine 203 of cyclophilin D is critical for cyclophilin D activation of the mitochondrial permeability transition pore. J. Biol. Chem. *286*, 40184–40192.

Nicolli, A., Basso, E., Petronilli, V., Wenger, R.M., and Bernardi, P. (1996). Interactions of cyclophilin with the mitochondrial inner membrane and regulation of the permeability transition pore, and cyclosporin A-sensitive channel. J. Biol. Chem. *271*, 2185–2192.

Petronilli, V., Costantini, P., Scorrano, L., Colonna, R., Passamonti, S., and Bernardi, P. (1994). The voltage sensor of the mitochondrial permeability transition pore is tuned by the oxidation-reduction state of vicinal thiols. Increase of the gating potential by oxidants and its reversal by reducing agents. J. Biol. Chem. *269*, 16638–16642.

Petronilli, V., Penzo, D., Scorrano, L., Bernardi, P., and Di Lisa, F. (2001). The mitochondrial permeability transition, release of cytochrome c and cell death. Correlation with the duration of pore openings in situ. J. Biol. Chem. *276*, 12030–12034.

Petronilli, V., Šileikyte, J., Zulian, A., Dabbeni-Sala, F., Jori, G., Gobbo, S., Tognon, G., Nikolov, P., Bernardi, P., and Ricchelli, F. (2009). Switch from inhibition to activation of the mitochondrial permeability transition during hematoporphyrin-mediated photooxidative stress. Unmasking pore-regulating external thiols. Biochim. Biophys. Acta *1787*, 897–904.

Poole, L.B. (2015). The basics of thiols and cysteines in redox biology and chemistry. Free Radic. Biol. Med. *80*, 148–157.

Porter, G.A., Jr., and Beutner, G. (2018). Cyclophilin D, somehow a master regulator of mitochondrial function. Biomolecules *8*, 176.

Prudent, J., Popgeorgiev, N., Bonneau, B., Thibaut, J., Gadet, R., Lopez, J., Gonzalo, P., Rimokh, R., Manon, S., Houart, C., et al. (2013). Bcl-wav and the mitochondrial calcium uniporter drive gastrula morphogenesis in zebrafish. Nat. Commun. *4*, 2330.

Prudent, J., Popgeorgiev, N., Bonneau, B., and Gillet, G. (2015). Bcl-2 proteins, cell migration and embryonic development: lessons from zebrafish. Cell Death Dis. *6*, e1910.

Rak, M., Tetaud, E., Godard, F., Sagot, I., Salin, B., Duvezin-Caubet, S., Slonimski, P.P., Rytka, J., and di Rago, J.P. (2007). Yeast cells lacking the mitochondrial gene encoding the ATP synthase subunit 6 exhibit a selective loss of complex IV and unusual mitochondrial morphology. J. Biol. Chem. *282*, 10853–10864.

Resmini, G., Rizzo, S., Franchin, C., Zanin, R., Penzo, C., Pegoraro, S., Ciani, Y., Piazza, S., Arrigoni, G., Sgarra, R., and Manfioletti, G. (2017). HMGA1 regulates the plasminogen activation system in the secretome of breast cancer cells. Sci. Rep. *7*, 11768.

Robb, E.L., Gawel, J.M., Aksentijević, D., Cochemé, H.M., Stewart, T.S., Shchepinova, M.M., Qiang, H., Prime, T.A., Bright, T.P., James, A.M., et al. (2015). Selective superoxide generation within mitochondria by the targeted redox cycler MitoParaquat. Free Radic. Biol. Med. *89*, 883–894.

Schinzel, A.C., Takeuchi, O., Huang, Z., Fisher, J.K., Zhou, Z., Rubens, J., Hetz, C., Danial, N.N., Moskowitz, M.A., and Korsmeyer, S.J. (2005). Cyclophilin D is a component of mitochondrial permeability transition and mediates neuronal cell death after focal cerebral ischemia. Proc. Natl. Acad. Sci. USA *102*, 12005–12010.

Schubert, A., and Grimm, S. (2004). Cyclophilin D, a component of the permeability transition-pore, is an apoptosis repressor. Cancer Res. *64*, 85–93.

Schultheiss, H.P., and Klingenberg, M. (1984). Immunochemical characterization of the adenine nucleotide translocator. Organ specificity and conformation specificity. Eur. J. Biochem. *143*, 599–605.

Steele, D.F., Butler, C.A., and Fox, T.D. (1996). Expression of a recoded nuclear gene inserted into yeast mitochondrial DNA is limited by mRNA-specific translational activation. Proc. Natl. Acad. Sci. USA *93*, 5253–5257.

Szabó, I., and Zoratti, M. (2014). Mitochondrial channels: ion fluxes and more. Physiol. Rev. *94*, 519–608.

Urbani, A., Giorgio, V., Carrer, A., Franchin, C., Arrigoni, G., Jiko, C., Abe, K., Maeda, S., Shinzawa-Itoh, K., Bogers, J.F.M., et al. (2019). Purified F-ATP synthase forms a Ca^{2+}-dependent high-conductance channel matching the mitochondrial permeability transition pore. Nat. Commun. *10*, 4341.

von Stockum, S., Giorgio, V., Trevisan, E., Lippe, G., Glick, G.D., Forte, M.A., Da-Rè, C., Checchetto, V., Mazzotta, G., Costa, R., et al. (2015). F-ATPase of Drosophila melanogaster forms 53-picosiemen (53-pS) channels responsible for mitochondrial Ca2+-induced Ca2+ release. J. Biol. Chem. *290*, 4537–4544.

Wach, A., Brachat, A., Pöhlmann, R., and Philippsen, P. (1994). New heterologous modules for classical or PCR-based gene disruptions in Saccharomyces cerevisiae. Yeast *10*, 1793–1808.

Woodfield, K., Rück, A., Brdiczka, D., and Halestrap, A.P. (1998). Direct demonstration of a specific interaction between cyclophilin-D and the adenine nucleotide translocase confirms their role in the mitochondrial permeability transition. Biochem. J. *336*, 287–290.

STAR★METHODS

KEY RESOURCES TABLE

REAGENT or RESOURCE	SOURCE	IDENTIFIER
Antibodies		
ATP synthase Immunocapture kit	Abcam	Cat# ab109715
Mouse monoclonal anti-β subunit	Abcam	Cat# ab14730; RRID: AB_301438
Mouse monoclonal anti-b subunit	Abcam	Cat# ab117991; RRID: AB_10901555
Mouse monoclonal anti-OSCP subunit	Abcam	Cat# ab110276; RRID: AB_10887942
Mouse monoclonal anti-OSCP subunit	Santa Cruz Biotechnology	Cat# sc-365162; RRID: AB_10709316
Mouse monoclonal anti-SDHA	Santa Cruz Biotechnology	Cat# sc-166947; RRID: AB_10610526
Rabbit polyclonal anti-ATP synthase gamma	ThermoFisher Scientific	Cat# PA5-29975; RRID: AB_2547449
Rabbit polyclonal anti-f subunit	Abcam	Cat# ab103951; RRID: AB_10711131
Rabbit polyclonal anti-ATP5L (g)	Abcam	Cat# ab126181; RRID: AB_11129974
polyclonal antibody anti-ATP5I (e)	Abcam	Cat# ab122241; RRID: AB_11127890
Mouse monoclonal anti-vinculin	Sigma-Aldrich	Cat# V4505; RRID: AB_477617
Mouse monoclonal anti-prohibitin	Lab Vision	Cat# MS-261-P1; RRID: AB_61896
Rabbit monoclonal anti-GAPDH	Cell Signaling	Cat# 2118; RRID: AB_561053
Mouse monoclonal anti-cyclophilinF (CyPD)	Abcam	Cat# ab110324; RRID: AB_10864110
Rabbit polyclonal anti-ATP synthase gamma	GeneTex	Cat# GTX114275; RRID: AB_10726795
Rabbit polyclonal anti-TOM20	Santa Cruz Biotechnology	Cat# sc-11415; RRID: AB_2207533
Bacterial and Virus Strains		
XL1-Blue Supercompetent Cells	Agilent	200236
One Shot™ TOP10 Chemically Competent *E. coli*	ThermoFisher Scientific	C404010
Chemicals, Peptides, and Recombinant Proteins		
Digitonin	Merck (Sigma-Aldrich)	D141
Oligomycin-A	Millipore	495455
Rotenone	Sigma-Aldrich	R8875
Antimycin A	Sigma-Aldrich	A8674
carbonylcyanide-p-trifluoromethoxyphenyl hydrazine (FCCP)	Merck (Sigma-Aldrich)	C2920
Cyclosporin A	Sigma-Aldrich	C3662
Calcium green-5N	ThermoFisher Scientific (Invitrogen)	C3737
Pyruvate Kinase	Merck (Sigma-Aldrich)	P1506
Lactate dehydrogenase (LDH)	Merck (Sigma-Aldrich)	L2625
Phosphoenolpyruvate	Sigma-Aldrich	P7002
MitoParaquat	Caymanchem	1821370-28-8
Diamide	Sigma-Aldrich	D3648
Phenylarsine oxide	Sigma-Aldrich	P3075
ATP	Sigma-Aldrich	A26209
NADH, Grade II disodium salt	Roche	10128023001
Calcium ionophore (ETH129)	Sigma-Aldrich	21193
Pyruvic Acid	Sigma-Aldrich	P-5280
Tungsten M-10 Microcarrier 0.7 μM	BIO-RAD	1652266
Alamethicin from Trichoderma viride	Sigma-Aldrich	A4665
Iodoacetamide	Merck (Sigma-Aldrich)	I6125
Ionomycin calcium salt from Streptomyces conglobatus	Sigma-Aldrich	I0634
1,4-Dithiothreitol	Merck (Sigma-Aldrich)	10708984001

(*Continued on next page*)

Continued

REAGENT or RESOURCE	SOURCE	IDENTIFIER
Sequencing Grade Modified Trypsin	Promega	V5111
Critical Commercial Assays		
Cell Titer 96® Aqueous One Solution	Promega	G3580
DeadEnd Fluorimetric TUNEL system	Promega	G3250
Experimental Models: Cell Lines		
HEK293T/17	ATCC	CRL-11268
Experimental Models: Organisms/Strains		
B6J mice	Charles River	N/A
Wild-type Zebrafish AB strain	Zebrafish Facility at University of Padova	N/A
MR6, *MATa ade2-1 his3-11,15 trp1-1 leu2-3,112 ura3-1 CAN1 arg8::HIS3* [r^+]	(Rak et al., 2007)	N/A
NB40-3C, *MATa lys2 leu2-3, 112 ura3-52 his3ΔHinDIII arg8::hisG, rho+ cox2-62* [r^+ *cox2-62*]	(Steele et al., 1996)	N/A
DFS160, *MATa leu2D ura3-52 ade2-101 arg8:: URA3 kar1-1* [r^0]	(Steele et al., 1996)	N/A
RKY149, *MATa ade2-1 his3-11,15 trp1-1 leu2-3,112 ura3-1 CAN1 arg8::HIS3* [r^+ *atp9-C65S*]	This study	N/A
RKY148, *MATa leu2D ura3-52 ade2-101 arg8:: URA3 kar1-1* [r^{-S} *atp9-C65S COX2*]	This study	N/A
RKY26, *MATa ade2-1 his3-11,15 trp1-1 leu2-3,112 ura3-1 CAN1 arg8::HIS3* [r^+ *atp9::ARG8m*]	(Bietenhader et al., 2012)	N/A
Yeast Parental Strain BY4743	Thermo BioScientific	YSC1050
Oligonucleotides		
sgRNA sequence: human OSCP GATGAGTGTCCATCGCGGAG	This study	N/A
ssDNA sequence: human OSCP, ACTCTGGCAGATTTGCTTGCTGAAAATGGTCGATTAAGCA ATACCCAAGGAGTCGTTTCTGCCTTTTCTACCATGATGAGTGTC CATCGCGGAGAAGTACCTAGCACAGTGACCTCTGCATCTGTAAGT AACGGGTTGTTGCTGCTGTGTTTGCCTTGATATTACATGTGTCA CCTTTTGCAGGAAGAAAAGGGAAAAA	This study	N/A
sgRNA sequence: human CyPD CCGACCCGCGCCCGCGATGC	This study	N/A
see Table S2		
Recombinant DNA		
pFA6-kanMX4	(Wach et al., 1994),	N/A
pFL38-URA	(Bonneaud et al., 1991),	N/A
pFL38-URA-ATP1	This study	N/A
pFL38-URA-ATP3	This study	N/A
pMOS-ATP9 plasmid	(Godard et al., 2011)	N/A
pJM2	(Bonnefoy and Fox, 2001)	N/A
pRK83	This study	N/A
pX330-U6-Chimeric_BB-CBh-hSpCas9	Addgene	42230
pcDNA3.1(+)Neo	Addgene	N/A
pcDNA3.1-ATP5O	This study	N/A
Software and Algorithms		
ImageJ	National Institutes of Health (NIH)	https://www.imagej.nih.gov/ij/download.html
GraphPad	GraphPad	https://www.graphpad.com
MaxQuant software package (version 1.5.1.2)	(Cox and Mann, 2008)	N/A
Other		
PicoFrit capillary column	New Objective	N/A
Aeris Peptide 3.6 μm XB-C18	Phenomenex	N/A

RESOURCE AVAILABILITY

Lead Contact

Further information and requests for resources and reagents should be directed to and will be fulfilled by the Lead Contact Paolo Bernardi (paolo.bernardi@unipd.it).

Materials Availability

Reagents generated in this study will be made available on request, but we may require a completed Materials Transfer Agreement.

Data and Code Availability

Data are available upon request.

EXPERIMENTAL MODEL AND SUBJECT DETAILS

HEK293 cells

HEK293 cells were grown in Dulbecco's modified Eagle's medium (DMEM) supplemented with 10% fetal bovine serum, 2 mM glutamine, 1 mM sodium pyruvate and 100 μg/ml penicillin and streptomycin at 37°C in a humidified atmosphere containing 5% CO_2.

Mice

The study employed 3 to 4 months-old B6J female mice (Charles River). All mice were housed on a 12:12 h light:dark cycle at 25°C. All animal procedures were in accordance with the animal care committee at University of Padova and the Italian ministry of health.

Zebrafish

Wild-type adult zebrafish were maintained in aerated, 28°C-conditioned saline water under a 13-h light/11-h dark cycle and fed according to standard protocols. All protocols and manipulations with zebrafish were approved by the Ethics Committee of the University of Padova and authorized by the Italian Ministry of Health.

METHOD DETAILS

Generation of HEK293 OSCP C141S and CyPD KO cell lines

The CRISPR/Cas9 system was used to alter the specific codon in exon 5 of the human OSCP (hOSCP) gene specifying Cys141 to Ser. This site was targeted by use of a guide RNA (gRNA; gatgagtgtccatcgcggag) subcloned into the BbsI site of px330 (Addgene). Repair single-stranded DNA (ssDNA) mediating Cys141 replacement by Ser was ACTCTGGCAGATTTGCTTGCTGAAAATGGTCGAT TAAGCAATACCCAAGGAGTCGTTTCTGCCTTTTCTACCATGATGAGTGTCCATCGCGGAGAAGTACCT**A**GCACAGTGACCTCTGCAT CTGTAAGTAACGGGTTGTTGCTGCTGTGTTTGCCTTGATATTACATGTGTCACCTTTTGCAGGAAGAAAAGGGAAAAA. The underlined, boldface residue mediates an amino acid change. HEK293T cells were grown in DMEM supplemented with 10% FBS and transfected at 70% confluency in six-well plates with 6 μl Lipofectamine 2000 with px330 hOSCP, 7 μg px330 hOSCP, 7 μg pAAV Syn-GFP (Addgene), 20 μM ssDNA. Following 3 days of growth, transfected cells were subjected to FAC sorting and single cells placed in individual wells of a 96-well plate. Individual colonies were subsequently transferred to six-well plates, DNA extracted and regions surrounding C141 sequenced to identify clones in which C141 remained or had been changed to S. Western blots of isolated mitochondria demonstrate that expression of OSCP is unchanged. HEK293T cells harboring the OSCP Cys141 to Ser mutation were put into a *CYPD* null background using CRISPR/Cas9 and Non-homologous end joining. Cells were transfected with pX330 containing a guide RNA (CCGACCCGCGCCCGCGATGC) to CYPD and further processed as outlined above.

Injection of zebrafish embryos

To verify the effects of OSCP C138S *in vivo*, zebrafish OSCP was cloned into pcDNA3.1 digested with KpnI and ApaI, using following primers: ATP5O FOR: 5′- CCGGTACCATGGCAGCGCTTGGAGTGGG and ATP5O REV: 5′- CCGGGCCCTTAGGTATCCCTGAT CAGC. Quick Change Lightning site-directed mutagenesis kit was used to introduce the C > S substitution by using following primers: ATP5O REV: 5′- GAGGTCACA**A**GCTCAGTCACC and ATP5O FOR: 5′- GGTGACTGAGC**T**TGTGACCTC. Mutation was confirmed by sequencing. Fertilized wild-type zebrafish embryos were injected at one-cell stage with 35 ng/μl of pcDNA3.1 plasmid harboring wild-type or OSCP C138S.

Generation of yeast C > S mutants

S. cerevisiae wild-type (BY4743) was purchased by Thermo Scientific. Deletion of ATP1 and ATP3 was carried out singularly by homologous recombination with the KanMX cassette of the pFA6-kanMX4 vector, using following primers: ATP1 FOR:5′-CAAGAA CAGTAACAAAATAAATAAAAAAAACACGCACATATAATACAGCTGAAGCTTCGTACGC and ATP1 REV: 5′-TTTTTGAGACGTACCT TATATTCATTTTTATTTTTTTAGTTCACAGCATAGGCCACTAGTGGATCTG; ATP3 FOR: 5′-GAAACAATTGAAGACGAGCAGTAA ACATTATTTTATTTAGTAGTCCAGCTGAAGCTTCGTACGC and ATP3 REV:5′-CAAAAACAACGTCAAATAAAGAGGCAATGCAG

GGTGATTTTTTTAGCATAGGCCACTAGTGGATCTG. Briefly, fresh liquid BY4743 cultures with an OD600 of about 0.6 were harvested, washed with sterile H2O and suspended in 100 mM LiAc solution for 15 min at 30°C. Then, cells were suspended in 25% PEG 3350 (50% w/v), 100 mM LiAc, 20 μg/ml DNA carrier and 10 μl PCR product, incubated 30 min at 30°C and then 20 min at 42°C. Cells were then grown for 3 h in YPD (2% glucose), washed twice and finally plated on YPD agar medium containing G418 (200 μg/ml). Colonies were checked for the presence of the deletion using a semiquantitative PCR and appropriate primers. For the cloning of ATP1 and ATP3 genes, pFL38-URA vector was digested with KpnI and BamHI and the target gene was amplified using primers that include upstream and downstream regulatory sites: ATP1 FOR: 5′-CACGACGTTGTAAAACGACGGCCAGTGAATTC GAGCTCGGTACCCCAATTCACTTTCTGAATAAG, ATP1 REV: 5′-TTACGCCAAGCTTGCATGCCTGCAGGTCGACTCTAGAG GATCCCCGGGTTATTGTTTGGCTGCAC; ATP3 FOR: 5′-CACGACGTTGTAAAACGACGGCCAGTGAATTCGAGCTCGGTACCCT GAATAGGAGCTGTCGCTAG,ATP3 REV:5′-TTACGCCAAGCTTGCATGCCTGCAGGTCGACTCTAGAGGATCCCCGGATATATACT TCGTCTCATC. Quick Change Lightning site-directed mutagenesis kit was used to introduce C > S substitution in each gene using following primers: ATP1 FOR: 5′-GAAACTTTACT**C**TGTTTACGTTGC, ATP1 REV: 5′-GCAACGTAAACA**G**AGTAAAGTTTC; ATP3 FOR: 5′-TAAGGGGTTGT**C**TGGTTCTATCC, ATP3 REV: 5′-GGATAGAACCA**G**ACAACCCCTTA. Mutations were confirmed by sequencing. One-step transformation protocol was used to transform the wild-type or C > S gene into corresponding deleted strain. Δatp1 and Δatp3 diploids were singularly transformed with pFL38-URA vectors carrying wild-type or C > S gene and resulting clones were grown in 1% potassium acetate medium for sporulation. Haploids were plated in selection agar media (YPD + G418, Drop-out -URA) and properly selected. The generation of homoplasmic atp9-C65S mutant was carried out by *in vitro* mutagenesis followed by biolistic transformation into the ρ^0 mitochondria of atp9-C65S gene and its recombination into the ATP9 locus of ρ^+ mitochondria. The Quik-Change XL Site-directed Mutagenesis Kit of Stratagene and the following mutagenic oligonucleotides were used to introduce the mutation into the ATP9 gene sequence on pMOS-ATP9 plasmid (modified base in boldface): 5′CGCCTTATCAGAAGCTACAGGTTT ATTCTCATTAATGGTTTCATTCTTATTATTATTCGGTG3′ and 5′ CACCGAATAATAATAAGAATGAAACCATTAATGAGAATAAACCTG TAGCTTCTGATAAGGCG 3′ (Godard et al., 2011). The mutated ATP9 fragment was released with BamHI-XbaI digestion and ligated at the same sites with pJM2. This plasmid contains the yeast mitochondrial COX2 gene as a marker for mitochondrial transformation. The resulting pRK83 plasmid was introduced by co-transformation with the nuclear selectable LEU2 gene containing plasmid Yep351 into the ρ^0 strain DFS160 by microprojectile bombardment using a biolistic PDS-1000/He particle delivery system (Bio-Rad) as described. Mitochondrial transformants were identified among the Leu+ nuclear transformants by their ability to produce respiring clones when mated to the non-respiring NB40-3C strain (MATa lys2 leu2-3, 112 ura3-52 his3ΔHinDIII arg8::hisG, ρ^+ cox2-62) bearing a deletion in the mitochondrial COX2 gene. The resulting clones (r- synthetic RKY148) were crossed to strain RKY26 (Bietenhader et al., 2012) with a WT nucleus and in which the ATP9 gene is replaced by ARG8m (atp9::ARG8m). In these crosses the atp9-C65S genes replaced by mtDNA recombination the ARG8m marker, resulting in a strain with complete (ρ^+) mtDNA carrying the atp9-C65S mutation, RKY149. The presence of mutation was verified by DNA sequencing of the amplified atp9-C65S gene.

Preparation of isolated mitochondria from HEK293 cells, mouse liver, and yeast

Isolation of mitochondria from HEK293 cells was performed as follows. HEK293 cells were collected with a cell scraper in cold PBS and spun at 500 x *g* for 5 min. The pellet was homogenized with a Teflon pestle in cold isolation buffer (IB) containing 250 mM sucrose, 10 mM Tris-HCl, 0.1 mM EGTA-Tris, pH 7.4 on ice in a glass potter using a Teflon pestle. Cell suspension was spun at 500 x *g* for min, surnatant was collected and centrifuged at 7,000 x *g* for 15 min at 4°C. Mitochondrial pellet was washed once with IB and spun down again. Protein concentration was determined with the BCA method. Isolation of mitochondria from mouse liver was performed as follows. Mouse liver was cut into small pieces in cold IB and homogenized with a rotating Teflon pestle. Homogenate was spun at 700 x *g* for 10 min at 4°C, surnatant was collected and spun at 7,000 x *g* for 10 min at 4°C to precipitate mitochondria. Mitochondrial pellet was washed with IB and spun down at 9,400 x *g* for 5 min. Protein concentration was determined with Biuret method. Yeast cells were cultured aerobically in 50 mL of 1% yeast extract, 1% bacto-polypeptone (YP) medium containing 2% glucose at 30°C. An aliquot corresponding to an optical density (600 nm) of 2 was then added to 400 mL of YP medium supplemented with 2% galactose and incubated for 20 h at 30°C under rotation at 180 rpm, yielding about 4.0 g of yeast cells. Briefly, cells were washed, incubated for 15 min at 37°C in a 0.1 M Tris-SO_4 buffer (pH 9.4) supplemented with 10 mM dithiothreitol (DTT) and washed once with 1.2 M Sorbitol, 20 mM Pi pH 7.4. Yeast cells were then suspended in the same buffer and incubated for 45 min at 30°C with 0.4 mg/g of cells of zymolyase 100T to form spheroplasts. The latter were washed once with sorbitol buffer and homogenized in 0.6 M Mannitol, 10 mM Tris-HCl, pH 7.4 and 0.1 mM EDTA-Tris with a Potter-Homogenizer. The homogenate was centrifuged for 5 min at 2,000 x g, the supernatant was collected and centrifuged for 10 min at 12,000 x g. The resulting mitochondrial pellet was suspended in mannitol buffer and protein concentration was determined from the A280 of SDS-solubilized mitochondria.

Ca^{2+} Retention Capacity (CRC)

Mitochondrial Ca^{2+} uptake was evaluated with Calcium Green-5N (Molecular Probes) fluorescence using a Fluoroskan Ascent FL (Thermo Electron) plate reader in mouse liver mitochondria (MLM), and permeabilized HEK293 cells. Two hundreds μg of MLM were resuspended in 250 mM sucrose, 10 mM MOPS-Tris, 5 mM glutamate/2.5 mM malate, 10 μM EGTA-Tris, 0.5 μM Ca^{2+} Green-5N, pH 7.4. The amount of Pi, Vi, DIA and PAO is specified in figure legends. Wild-type MLM were subjected to 5 μM Ca^{2+} pulses, while CyPD KO MLM to 10 μM Ca^{2+} pulses. CRC in permeabilized cells was performed as follows. HEK293 cells were detached with 0.05% trypsin, spun at 500 x *g* for 5 min and washed with PBS. Cells were resuspended in 130 mM KCl, 10 mM

MOPS-Tris, 0.1 mM EGTA-Tris, pH 7.4 (B1), counted and spun down at 500 x *g* for 5 min. The pellet was resuspended in 130 mM KCl, 10 mM MOPS-Tris, 1 mM EGTA-Tris, pH 7.4 to a final concentration of 20 × 10^6 cells/ml and 100 μM digitonin was added. Cells were let incubating with digitonin for 10 min on ice and were checked for permeabilization with Trypan blue. The reaction was stopped with B1, cells were centrifuged at 500 x *g* for 5 min and washed with B1. The final pellet was resuspended in 130 mM KCl, 10 mM MOPS-Tris, pH 7.4 to a final concentration of 10 × 10^6 cells/ml and supplemented with 5 mM succinate, 2 μM rotenone and 0.5 μM Ca^{2+} Green-5N. The amount of Pi is indicated in figure legends. Permeabilized wild-type and OSCP C141S cells were subjected to 5 μM Ca^{2+} pulses, while cells in CyPD KO background to 10 μM Ca^{2+} pulses. Fifty μg of yeast isolated mitochondria were resuspended in 250 mM sucrose, 10 mM Tris-MOPS, 1 mM NADH, 10 μM EGTA-Tris, 2 mM Pi-Tris, 5 μM ETH129, 1 μM Ca^{2+} Green-5N, pH 7.4 and 0.5 mg/ml bovine serum albumin. Yeast mitochondria were subjected to trains of 10 μM Ca^{2+} pulses.

ATP hydrolysis

ATPase activity was measured in yeast isolated mitochondria using a 96-well clear plate in a final volume of 0.2 ml. Mitochondria were suspended at 10 μg/ml in 50 mM KCl, 50 mM Tris-HCl, 30 mM sucrose, 4 mM $MgCl_2$, 2 mM EGTA, pH 7.4 supplemented with 4 units/ml pyruvate kinase, 3 units/ml lactate dehydrogenase, 4 mM phosphoenolpyruvate, 2 mM ATP, 0.2 mM NADH, 50 μM sodium decavanadate and 10 μM alamethicin. Absorbance at 340 nm was read in presence and absence of 10 μM oligomycin.

Oxygen consumption rate

Oxygen consumption rate in adherent cells was measured with an XF24 Extracellular Flux Analyzer (Seahorse Bioscience). Briefly, HEK293 cells were seeded in XF24 microplates coated with 0.01% poly-L-lysine (Sigma) at 6 × 10^4 cells/well for wild-type, OSCP C141S and CyPD KO cells and at 10 × 10^4 cells/well for CyPD KO + OSCP C141S cells in 200 μL DMEM (high glucose, glutamine, and sodium pyruvate, Life Technologies) and let growing at 37°C in a 5% CO_2 humidified incubator for 24h. Before initiating the assay, the growth medium was replaced with Seahorse medium (DMEM-Sigma D5030) supplemented with 143 mM NaCl, 25 mM glucose, 10 mM sodium pyruvate, 2 mM glutamine and 15 mg/L phenol red. Cells were incubated at 37°C for 30 min to allow temperature and pH equilibration. After an OCR baseline measurement, 1 μg/ml oligomycin, twice of 50 nM FCCP and 1 μM rotenone plus 1 μM antimycin were sequentially added to each well. OCR values were subtracted for the rotenone and antimycin insensitive respiration and where indicated were normalized for μg of protein measured by BCA method.

Immunoprecipitation and Western Blot

Immunoprecipitation of F-ATP synthase was performed in wild-type and CyPD KO MLM. Briefly, 500 μg of mitochondria were resuspended in 250 mM sucrose, 10 mM MOPS-Tris, 5 mM glutamate/2.5 mM malate, 0.5 mM Pi, 10 μM EGTA-Tris, pH 7.4, in a final volume of 500 μL and let incubate for 10 min at RT in presence or not of DIA (2 or 5 mM). Mitochondria were centrifuged at 9,400 x *g* for 5 min at 4°C and resuspended in 50 μL of 1M aminocaproic acid, 50 mM Bis-Tris, 0.5 mM Pi, pH 7.0. Mitochondria were solubilized with a digitonin-to-protein ratio of 1 g/g (Sigma) and centrifuged at 100,000 x *g* for 25 min at 4°C. Surnatant was collected and 10 μL of protein G-agarose beads cross-linked with monoclonal antibodies against F-ATP synthase (ATP synthase immunocapture kit, abcam) were added and let incubating overnight at 4°C. Beads were centrifuged at 500 x *g* for 5 min at 4°C and washed twice with PBS supplemented with 0.01% n-dodecyl β-D-maltoside (DDM). Beads were incubated with Laemmli buffer (1X) without β-mercaptoethanol for 15 min, spun down at 500 x *g* for 5 min and the resulting surnatant (eluate) was collected (this procedure was repeated three times). Samples were boiled at 98°C for 5 min and subjected to a SDS-PAGE followed by western blotting against OSCP (sc-365162, Santa Cruz Biotechnology), b and β subunits of F-ATP synthase. The immunoprecipitation of OSCP subunit was carried out in isolated mitochondria from HEK293 cells. Briefly, 250 μg of mitochondria were resuspended in 250 mM sucrose, 10 mM MOPS-Tris, 5 mM succinate, 0.1 mM Pi, 10 μM EGTA-Tris, 2 μM rotenone, pH 7.4, in a 250 μL final volume and incubated 18 min at RT with or without 0.3 mM DIA. Mitochondria were centrifuged at 7,000 x *g* for 15 min at 4°C and resuspended in 250 μL IP buffer (15 mM Tris-HCl, 2 mM EDTA-Tris, 1.8 mM EGTA-Tris, 0.1 mM Pi, 0.5% (v/v) Triton X-100, 0.25% (w/v) SDS, 0.005% BSA supplemented with 1 μg OSCP antibody (ab110276) and let incubating for 2 h at 4°C. Finally, 30 μL dynabeads protein G (Invitrogen) were added to sample and let incubating overnight at 4°C. After three washes with IP buffer devoid of SDS, the elution was carried out for 30 min in 25 μL Laemmli buffer (1X) without β-mercaptoethanol at 37°C. The collected fractions were heated at 98°C for 5 min and subjected to a SDS-PAGE followed by western blotting against OSCP subunit. For mass spectrometry analysis, the protocol included following variations. One-milligram of wild-type or OSCP C > S isolated mitochondria was incubated in presence or absence of 0.6 mM DIA and the OSCP IP elution was subjected to a 12% SDS-PAGE that was stained with a Coomassie blue solution. For the western blot analysis in zebrafish, injected embryos (about 50) at 72 h post-fertilization (hpf) were rinsed in 0.2 mL of Ringer solution, containing 1% Triton X-100, protease and phosphatase inhibitor cocktail (Sigma), and kept on ice for 20 min. Then, embryos were passed in a Potter homogenizer and protein extracts were cleared by centrifugation at 18,000 × *g* for 20 min at 4°C. Cleared lysates were solubilized in Laemmli buffer and subjected to SDS-PAGE and immunoblotting. All western blots were performed in PBS-Tween (0.1%) containing 5% non-fat dry milk. Following antibodies were used for murine and human samples: anti-SDHA (sc-166947, Santa Cruz Biotechnology), anti-β (ab14730), anti-γ (PA5-29975, ThermoFisher), anti-b (ab117991, abcam), anti-OSCP (ab110276, abcam), anti-f (ab200715, abcam), anti-g (ab126181, abcam), anti-e (ab122241, abcam), anti-vinculin (V4505, Sigma), anti-prohibitin (MS-261-P1, NeoMarkers), anti-GAPDH (2118, Cell Signaling) and anti-CyPD (ab110324, abcam). For Western Blot in zebrafish, anti-OSCP (sc-365162, Santa Cruz Biotechnology), anti-γ (GTX114275, GeneTex) were used.

In-gel trypsin digestion and LC-MS/MS analysis

Bands corresponding to the putative protein complex at 41 kDa were excised from the gel and digested with trypsin as described in (Resmini et al., 2017). Samples were subjected to LC-MS/MS analysis using a LTQ-Orbitrap XL mass spectrometer (Thermo Fisher Scientific) coupled online with a nanoHPLC Ultimate 3000 (Dionex – Thermo Fisher Scientific). Peptides were separated on a picofrit capillary column (11 cm, 75 μm I.D., New Objective) packed in house with C18 material (Aeris Peptide 3.6 μm XB-C18, Phenomenex) using a linear gradient of acetonitrile/0.1% formic acid from 3% to 40% in 20 min. A Top3 data dependent acquisition method was used for the analysis: a full MS scan was performed at high resolution (60000) on the Orbitrap, followed by MS/MS scans on the 3 most intense ions at low resolution in the Linear Ion Trap. Data were analyzed with the MaxQuant software package [version 1.5.1.2; J. Cox, M. Mann, Nat. Biotechnol. 26, 1367 (2008)] against the Human section of the Uniprot database (version 20141201). Trypsin was set as digesting enzyme with up to 2 missed cleavages, carbamidomethylation was set as fixed modification and methionine oxidation as variable modification. Data were filtered to have a False Discovery Rate (FDR) < 0.01 both at peptide and protein level. The intensity relative to each identified protein was calculated by the software and used to estimate the abundance of OSCP in the different samples.

Cell death assay (LDH release)

HEK293T cells were maintained in DMEM (11995065, Life Technologies) supplemented with 10% FBS, 1% P/S, and cultured at 37°C in the presence of 5% CO_2. For cell death assay, HEK cells were seeded in 24-well plates at density of 5×10^4 cells/well. After 48h, cells were incubated in the presence or absence of 10 μM MitoPQ at 37 °C in a humidified incubator. Supernatant aliquots were collected after 24h of MitoPQ treatment, and the release of LDH was measured as described (Di Lisa et al., 2001). At the end of each experiment, cells were lysed with 1% Triton X-100 (Sigma) for 30 min, and supernatants were collected to evaluate the total amount of LDH. LDH enzymatic activity was evaluated spectrophotometrically by measuring the absorbance of nicotinamide adenine dinucleotide (Roche) at 340 nm, indicative of the reduction of pyruvate to lactate. The extent of cell death has been shown as the fold increase normalized to the DMSO treated wild-type cells.

Cell viability assay (MTS test)

HEK293 cells were seeded in 96-well plates at a density of 8×10^4 cells/well in DMEM (D5030, Life Technologies), supplemented with 3.7 g/L sodium bicarbonate, 1 g/L glucose, 2 mM L-glutamine, 1 mM sodium pyruvate, 1% P/S and 1% FBS and grown for 24 h at 37°C with 5% CO_2. Cells were then treated with indicated concentrations of DIA or 4 μM ionomycin for 90 min. Cell viability was evaluated with CellTiter 96® Aqueous One solution Cell Proliferation Assay (MTS) (Promega), by measuring absorbance at 490 nm, according to manufacturer's instructions. The extent of cell viability upon treatments was normalized to that of untreated control for each genotype.

Whole-mount immunofluorescence

Expression of wild-type and OSCP C138S was detected by whole-mount immunofluorescence in 72 hpf embryos injected as previously described (Giorgio et al., 2017). Briefly, embryos at 72 hpf were fixed for 3 h in 4% (w/v) paraformaldehyde (PFA) solution in PBS. After rehydration in methanol (from 100% to 25%) and washing in PBS, embryos were incubated in a permeabilization solution containing 10 μg/ml proteinase K in PBS supplemented with 0.1% Tween-20 for 40 min at room temperature. After 15 min fixation with 4% (w/v) PFA in PBS, samples were incubated in 1% (v/v) DMSO in PBS/Tween for 20 min at room temperature to block the permeabilization. After washings in PBS, embryos were incubated with primary antibodies diluted 1:100 in PBS/Tween (polyclonal rabbit anti-TOM20, Santa Cruz Biotechnology, and monoclonal mouse anti-OSCP (A-8), Santa Cruz Biotechnology) at 4°C for 72 h. After extensive washings in PBS, embryos were incubated for 48 h at 4°C with secondary antibodies (anti-mouse TRITC conjugated and anti-rabbit FITC conjugated, Dako) diluted 1:500 in PBS/Tween. Full Z stack images were collected with a NIKON H600L confocal microscope (20x objective) equipped with Laser 488 (excitation 488 nm and emission 520 nm) to visualize FITC and Laser 561 (excitation 561 nm and emission 620 nm) for TRITC.

TdT-mediated dUTP Nick-End Labeling (TUNEL) assay

To assess the effects of wild-type and OSCP C138S on apoptosis, TUNEL assay was performed on embryos at 72 hpf using a TUNEL kit protocol (Promega). Briefly, 4/5 embryos for each condition were fixed for 1 h with 4% PFA (w/v) in PBS solution. After three washes with PBS-Triton 0.1%, embryos were permeabilized for 30 min in PBS-Triton 0.15%. Then, embryos were pre-incubated with equilibration buffer (TUNEL kit, Promega) for 10 min and then, incubated for 1 h in the dark at 37°C in equilibration buffer supplemented with fluorescein-12-dUTP mix and rTdT enzyme (TUNEL kit, Promega). The reaction was stopped by incubating embryos in a solution containing 0.3 M NaCl, 0.03 M trisodium citrate, pH 7, for 20 min. Then, embryos were transferred onto glass slides, set in 0.8% low melting agarose, laterally oriented, and analyzed using a NIKON H600L confocal microscope equipped with Laser 488 (excitation 488 nm and emission 520 nm) to visualize GFP and a 40x objective. Apoptotic nuclei in the tail area were analyzed and counted using ImageJ software.

QUANTIFICATION AND STATISTICAL ANALYSIS

Data were analyzed and presented as mean ± standard deviation (SD) or standard error of the mean (SEM) in all figures. Pairs of data groups were analyzed with a two-tailed Student's t tests. In the case of more than two groups, one-way analysis of variance (ANOVA) followed by Bonferroni post hoc test was applied. Statistical significance was determined using GraphPad software. Results with a p value lower than 0.05 were considered significant; ***$p < 0.001$, **$p < 0.01$, *$p < 0.05$ compared to controls. Each experiment was repeated at least three times.